Title

**Increased fibrosis and impaired intratumoral accumulation of macromolecules in a murine model of pancreatic cancer co-administered with FGF-2**

Authors:

Satoshi Sakai[1], Caname Iwata[1], Yasuyuki Morishita[1], Kohei Miyazono[1], Mitsunobu R Kano[2,*]

Affiliations:

[1]Department of Molecular Pathology, Graduate School of Medicine, The University of Tokyo, 7-3-1 Hongo, Bunkyo-ku, Tokyo, 113-0033 Japan, and [2]Department of Pharmaceutical Biomedicine, Graduate School of Medicine, Dentistry, and Pharmaceutical Sciences, Okayama University, 1-1-1 Tsushima-Naka, Kita-ku, Okayama-shi, Okayama, 700-8530 Japan.

*Corresponding author

E-mail: mikano-tky@umin.net

**Abstract**

Pancreatic cancer is notorious for its poor prognosis. The histopathologic characteristic of pancreatic ductal adenocarcinoma (PDAC), which is the most common type, is fibrosis within tumor tissue. Although fibrosis within tumor tissue is thought to impede drug therapy by interfering with the intratumoral accumulation of anti-tumor drugs, this hypothesis has yet to be proven directly in preclinical models. Here, we evaluated the effect of enhanced fibrosis on intratumoral accumulation of macromolecular drugs by increasing fibrosis in a murine tumor model of subcutaneously xenografted BxPC-3, a human PDAC cell line. When fibroblast growth factor-2 (FGF-2) was co-administered upon BxPC-3 inoculation, stromal fibrotic area was increased and was characterized by augmented murine collagen accumulation compared to inoculation of BxPC-3 alone. We discovered that the intratumoral accumulation of intravenously administrated fluorescein isothiocyanate-dextran of 2,000,000 Da (2 MDa) was significantly reduced in the FGF-2 co-administered tumors despite unaltered hyaluronan accumulation and pericyte coverage of the tumor neovasculature and increased lymphangiogenesis. The model established and analyzed in this study, characterized by increased fibrotic component, provides a preclinical animal model suited to predict the intratumoral accumulation of macromolecular drugs and to evaluate the efficacy of drugs targeting the tumor stroma.

**Keywords**

macromolecular drugs, drug distribution, pancreatic ductal adenocarcinoma, fibrosis, FGF-2

## Introduction

Pancreatic cancer is well known for its dismal prognosis. The cancer is often inoperable at diagnosis due to its highly metastatic and invasive nature. Therefore, chemotherapy is an important treatment modality for pancreatic cancer [1] although its efficacy to date is far from being satisfactory. Pancreatic ductal adenocarcinoma (PDAC) in particular, the most common type of pancreatic cancer, has a 5-year relative survival rate of 6% and a median survival rate of 6 months [1,2]. Marked fibrosis, or desmoplasia, which is a histological feature of PDAC [2], is considered to be a factor explaining the refractoriness of PDAC to chemotherapy. Fibrotic tissue within the tumor consists of several types of extracellular matrix (ECM) components, such as collagen, hyaluronan, and fibronectin [3]. Previous reports have shown that a decrease in ECM components within tumor models *in vivo* or *in vitro* results in enhanced intratumoral accumulation of anti-tumor drugs, especially of macromolecules [4–8]. However, no reports to date have demonstrated that an increase of ECM components limits intratumoral accumulation of macromolecules *in vivo*.

Difficulty in evaluating the effects of enhanced fibrosis on the intratumoral accumulation of anti-tumor drugs is a consequence of the lack of animal models in which the amount of fibrosis can easily be regulated and increased. Although xenografts of

established human tumor cell lines into immunodeficient animals is widely used as animal models of human tumors, fibrosis within xenograft tumor tissue is often diminished compared to clinical specimens [9,10]. We previously reported that the BxPC-3 subcutaneous xenograft model has some levels of fibrosis, greater in amount than that in most animal cancer models, but far less than that found in human pathologic specimens of the disease [11]. While some genetically engineered murine models of pancreatic cancer have marked fibrosis, researchers have to wait 6-9 months before the tumors grow large enough to analyze [2], and the degree of fibrosis cannot easily be modulated. Recently, we have shown that enhanced fibrosis may impair the intratumoral accumulation of drugs using a novel *in vitro* fibroblast three-dimensional culture model [12]. However, little is known about how to enhance fibrosis *in vivo* and its consequences.

Extent of fibrosis is known to correlate positively with fibroblast growth factor-2 (FGF-2) mRNA level in clinical pancreatic tumor specimens [13]. FGF-2 induces fibrosis by promoting the production of collagen and fibronectin in activated pancreatic stellate cells (PSCs) in humans, which are thought to be a major source of ECM in pancreatic cancer and chronic pancreatitis [14–16]. Moreover, FGF-2 neutralization has been shown to counteract the induction of fibronectin production in primary PSCs derived from clinical pancreatic cancer specimens by supernatants from pancreatic cancer cell

lines [17]. These findings suggest that FGF-2 may promote fibrosis in pancreatic cancer.

In this study, we report a novel way to enhance fibrosis by using xenografted BxPC-3 cells co-administered with FGF-2 in nude mice, and investigate whether enhanced fibrosis affects intratumoral accumulation of macromolecular drugs.

## Materials and Methods

*Cell and animal model*

The human pancreatic adenocarcinoma cell line BxPC-3 was obtained from the American Type Culture Collection (VA, USA) and cultured in RPMI 1640 medium (Life Technologies, CA, USA) with 10% fetal bovine serum (Hyclone, UT, USA) and 1% penicillin/streptomycin (Life Technologies). Male BALB/c-*nu/nu* mice, 4–6 weeks of age, were obtained from CLEA Japan (Tokyo, Japan), Sankyo Labo Service (Tokyo, Japan), and Charles River Laboratories, (Tokyo, Japan). All animal experimental protocols were performed in accordance with the policies of the Animal Ethics Committee of the University of Tokyo.

BxPC-3 subcutaneous xenograft model was established with a total of 1 x $10^6$ cells suspended in 200 μL of Matrigel (BD biosciences, CA, USA)/phosphate buffered saline (PBS) mixture (1:1) inoculated into the left flank of each mouse. To enhance fibrosis, 1 μg/mL of FGF-2 (Peprotech, NJ, USA) and 100 μg/ml of heparin (Novo Nordisk, Bagsvaerd, Denmark) were added in the cell suspension before inoculation. Three to four weeks after inoculation, the tumor-bearing mice were used for the experiments.

*Histological analysis*

Formalin-fixed, paraffin-embedded tumor samples were cut at a thickness of 4 μm and subjected to hematoxylin-eosin (HE) and AZAN staining. BZ-9000 (Keyence, Osaka, Japan) was used to observe the samples and obtain photographs. For quantification of AZAN positive areas, tile-scanned images were merged using BZ analyzer (Keyence) and then the proportion of AZAN positive areas was calculated by dividing intratumoral AZAN positive area (in pixels) by the whole tumor area (in pixels), using Adobe Photoshop Elements (Adobe Systems Incorporated, CA, USA) and ImageJ (National Institute of Health, MD, USA).

*Immunohistochemistry*

Harvested tumor samples were also immediately embedded in Optimal Cutting Temperature (OCT) compound (Sakura Finetek Japan, Tokyo, Japan) and frozen at -80°C. The frozen samples were cut at a thickness of 10 μm, briefly fixed with Mildform (Wako Pure Chemical Industries, Osaka, Japan), washed and air dried. The sections were then blocked with Blocking One (Nacalai Tesque, Kyoto, Japan) for 30 min at room temperature, and incubated with primary antibodies overnight at 4°C. The samples were then washed and incubated with the appropriate secondary antibodies for 1 hour at room

temperature. The secondary antibodies used in this study were anti-rat Alexa Fluor 488, anti-rat Alexa Fluor 594, anti-rabbit Alexa Fluor 488 and anti-rabbit Alexa Fluor 594 (all purchased from Life Technologies). After washing briefly, nuclei were stained with 1 μg/mL of 4,6-diamidino-2-phenylindole dihydrochloride (DAPI) (Life Technologies). The samples were observed using BZ-9000 or DMI6000 B AFC (Leica Microsystems, Wetzlar, Germany). The primary antibodies used in this study were that against platelet endothelial cell adhesion molecule-1 (PECAM-1; BD biosciences), α-smooth muscle actin (α-SMA; Sigma-Aldrich, MO, USA), and lymphatic vessel endothelial hyaluronan receptor-1 (LYVE-1; Abcam, Cambridge, UK). Intratumoral PECAM-1 positive areas and intratumoral PECAM-1/α-SMA double positive areas were quantified using Adobe Photoshop Elements and ImageJ by dividing intratumoral PECAM-1 positive areas (in pixels) by whole tumor areas (in pixels), or by dividing intratumoral double positive areas (in pixels) by PECAM-1 positive areas (in pixels), respectively, for tile-scanned images obtained and merged using BZ analyzer. For quantification of LYVE-1 positive lymphatic vessels, ten fields per sample were taken using DMI6000 B AFC and the average numbers of lymphatic vessels were counted. Frequency of lymphatic vessels with lumen was calculated by dividing the number of lymphatic vessels with conspicuous lumen by total number of lymphatic vessels.

*Evaluation of intratumoral hyaluronan accumulation*

For hyaluronan staining, formalin-fixed, paraffin-embedded samples were cut at a thickness of 4 μm, deparaffinized, washed, and blocked with Blocking One for 30 min at room temperature. After blocking, the samples were incubated with 2.5 μg/mL of biotinylated hyaluronan binding protein (biotin-HABP) (Hokudo, Sapporo, Japan) overnight at 4°C. The samples were then washed and incubated with 5 μg/mL of Alexa Fluor 488 streptavidin (Life Technologies) for 1 hour at room temperature. Nuclei were stained with 1 μg/mL of DAPI. For hyaluronidase treatment, some samples were washed with PBS (pH 5.5) just after blocking and incubated with 400 U/mL of hyaluronidase from bovine testes (Sigma-Aldrich) in PBS (pH 5.5) at 37°C for 2 hours. For quantification of hyaluronan accumulation, tile-scanned images were obtained and merged using BZ analyzer, and the average signal intensity in the tumor area was calculated using Adobe Photoshop Elements and ImageJ.

*Evaluation of intratumoral accumulation of FITC-dextran*

Analysis of intratumoral accumulation of fluorescein isothiocyanate (FITC)-dextran (average molecular weight 2 MDa) (Sigma-Aldrich) was done as follows. FITC-

dextran was dissolved in physiological saline (Otsuka Pharmaceutical, Tokyo, Japan) and its concentration was adjusted to 10 mg/mL. The solution was intravenously administered into tumor-bearing mice (200 μL per mouse). Six hours after administration, the tumor samples were harvested and immediately embedded in OCT compound and frozen at -80°C. These samples were cut at a thickness of 10 μm and fixed with Mildform for 5 min. Nuclei were stained with 1 μg/mL DAPI. BZ-9000 was used to observe the samples. For quantification of intratumoral accumulation of FITC-dextran, tile-scanned images were obtained and merged using BZ analyzer and then the average signal intensity in the tumor area was calculated using Adobe Photoshop Elements and ImageJ.

*Evaluation of hydroxyproline amount*

Amount of collagen was quantified by measuring hydroxyproline content. Hydrolysis of the samples was performed following a previous report [18] with minor modifications. Briefly, excised tumor samples were trimmed, weighed and homogenized in 20 volumes of 6 N hydrochloric acid (HCl) (w/v). Homogenized samples were transferred into polypropylene micro tubes with O-ring screw caps (Sarstedt, Numbrecht, Germany) and incubated overnight at 121°C. The residue was removed using Amicon Ultra-4 (10 k) (Millipore, MA, USA). 10 μL of each sample was transferred into a 96-

well plate (Thermo Fisher Scientific, MA, USA) and hydroxyproline content was measured using Hydroxyproline Assay Kit (Biovision, CA, USA), according to the manufacturer's protocol.

*Total RNA extraction and quantitative real-time RT-PCR*

Excised tumor samples were trimmed, cut into several small pieces and homogenized in Isogen (Nippon Gene, Tokyo, Japan) using Medimachine (Syntec International, Dublin, Ireland). Isolation of total RNA was performed according to the protocol for Isogen. Elimination of genome DNA in total RNA was performed using Nucleospin (Macherey-Nagel, Duren, Germany) according to the manufacturer's protocol. First-strand cDNA synthesis was performed using 1 μg of total RNA and PrimeScript Reverse Transcriptase (Takara Bio, Shiga, Japan).

Quantitative real-time RT-PCR was performed using FastStart Universal SYBR green master (Roche, Basel, Switzerland) and Step One Plus (Life Technologies). Primers used in this experiment were: GAAGGTGAAGGTCGGAGTC and GAAGATGGTGATGGGATTTC for human GAPDH, AGCCAGCAGATCGAGAACAT and TCTTGTCCTTGGGGTTCTTG for human COL1A1, TGCAGTGGCAAAGTGGAGATT and TGCCGTTGAATTTGCCGT for murine Gapdh,

and AACCCGAGGTATGCTTGATCT and CCAGTTCTTCATTGCATTGC for murine Col1a1.

*Statistical analysis*

The data were expressed as means ± standard error (SE). Statistical evaluation of the data was carried out by two-tailed, unpaired Student's t-test for comparison between two groups, using Microsoft Excel. Statistical significance was set at the level of $p < 0.05$.

**Results**

The FGF-2 co-administered BxPC-3 xenograft tumors harvested 3 weeks after inoculation showed markedly more fibrosis upon HE and AZAN staining compared to BxPC-3 xenografts without FGF-2 (Figure 1A). Indeed, the proportion of AZAN positive area was significantly increased with the co-administration of FGF-2 (Figure 1B). These findings indicate that FGF-2 enhanced fibrosis in the BxPC-3 subcutaneous xenograft model.

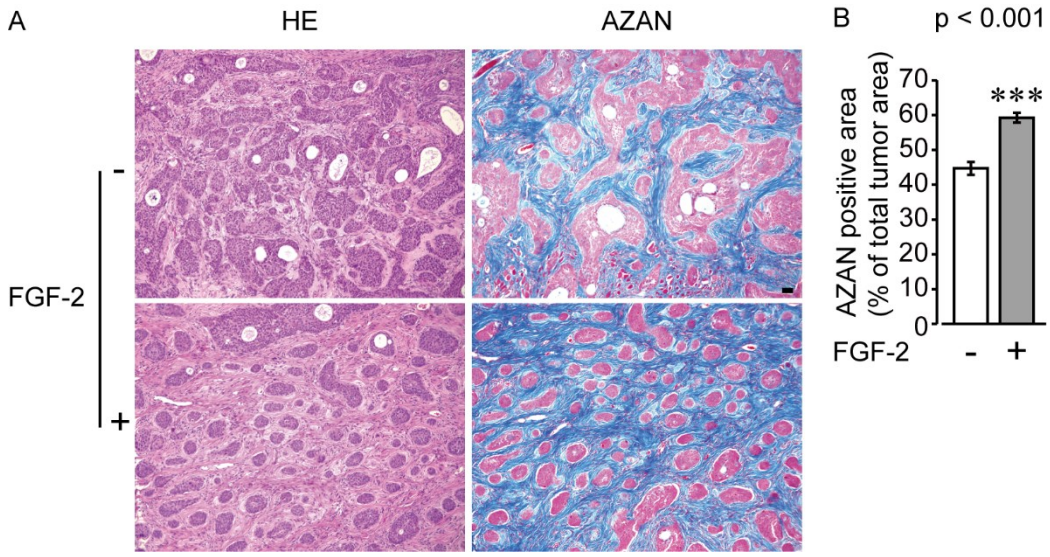


**Figure 1 FGF-2 increased tumor stroma in the BxPC-3 subcutaneous xenograft model.**
A: Representative photographs of HE and AZAN staining. FGF-2 markedly increased AZAN positive areas (AZAN staining, blue). scale bar: 50 μm
B: Quantification of the proportion of AZAN positive areas. FGF-2 significantly increased AZAN positive areas. error bars: mean ± SE, n =11 each, ***: $p < 0.001$

We next investigated possible components of the ECM contributing to increased fibrosis: collagen, the major component of ECM, and hyaluronan, which is known to

impair intratumoral drug accumulation in genetically-engineered mouse models of pancreatic adenocarcinoma [4,5]. We first measured hydroxyproline content, a surrogate index of collagen content. FGF-2 co-administration significantly increased hydroxyproline content of the BxPC-3 xenograft model (Figure 2A). To assess the origin of collagen, the mRNA expression of murine Col1a1 (mCol1a1) and human COL1A1 (hCOL1A1) was each quantified. The expression of murine collagen was significantly higher in the FGF-2 co-administered group (Figure 2B), while that of human was not significantly altered (Figure 2C), suggesting that the increased collagen content was not of BxPC-3 origin but rather host-derived.

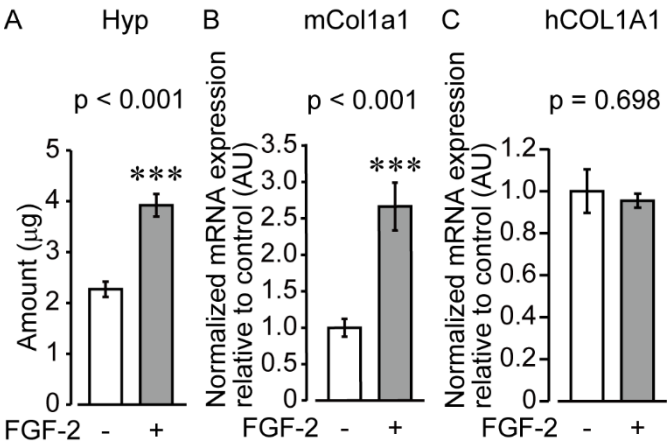


**Figure 2 FGF-2 increased collagen in the BxPC-3 model.**

A: Hydroxyproline (Hyp) content of tumor tissue. The amount was significantly higher in FGF-2 co-administered group. error bars: mean ± SE, n = 6 each, ***: $p < 0.001$

B: Expression level of murine Col1a1 (mCol1a1). FGF-2 significantly increased mCol1a1 expression. Data were normalized to mGAPDH and expressed as relative value to the average of control group. AU: arbitrary unit, error bars: mean ± SE, n = 11 and 9, respectively, ***: $p < 0.001$

C: Expression level of human COL1A1 (hCOL1A1). No significant difference was observed. Data were normalized to mGAPDH and expressed as relative value to the average of control group. AU: arbitrary unit, error bars: mean ± SE, n = 3 each.

For hyaluronan, accumulation was observed both in tumor stromal and

parenchymal areas by fluorescent immunostaining (Figure 3A) which was confirmed by hyaluronidase treatment (Figure 3B), but no significant difference was observed regardless of FGF-2 co-administration (Figure 3C). Thus, the enhanced fibrosis induced by FGF-2 co-administration in this model seems, at least partly, to be due to enhanced collagen production by host-derived stromal cells but independent of hyaluronan accumulation.

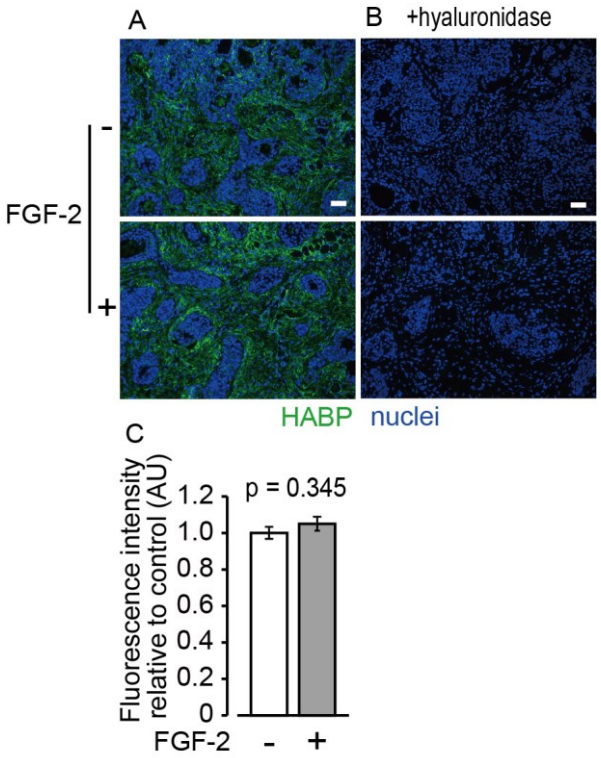


**Figure 3 FGF-2 did not affect intratumoral accumulation of hyaluronan**

A: Hyaluronan binding protein (HABP, green) detected hyaluronan. Nuclei were stained with DAPI (blue). B: Hyaluronan staining using different sections of the same samples as A. Hyaluronan staining using different sections of the same samples as A. Treatment with hyaluronidase almost completely abrogated the fluorescence signal (green), thus confirming successful staining of hyaluronan. Nuclei were stained with DAPI (blue). scale bars: 50 μm. C: Quantification of average fluorescence intensity of images as stained in A. Data were expressed as relative value to the average of control group. No difference was observed between the two groups. AU: arbitraty unit, error bars: mean ± SE, n = 5 each.

Using this newly established murine pancreatic cancer model with enhanced fibrosis, we asked whether enhanced fibrosis could impair intratumoral accumulation of

macromolecular drugs by using FITC-dextran (average molecular weight 2 MDa) as a tracer mimicking the kinetics of macromolecular drugs. As in our previous report [19], six hours after intravenous administration of FITC-dextran solution, the tumors were harvested and intratumoral accumulation of FITC-dextran analyzed. Fluorescence signal from FITC-dextran was significantly lower in FGF-2 co-administered xenografts than those without FGF-2 (Figure 4A and B). Intratumoral accumulation of FITC-dextran was thus diminished in FGF-2 co-administered xenografts.

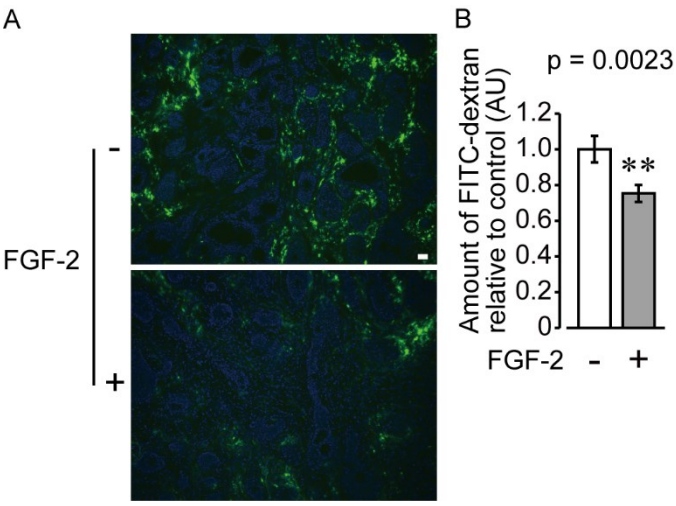


**Figure 4 FGF-2 reduced intratumoral accumulation of FITC-dextran (average molecular weight 2 MDa)**

A: Representative photographs of intratumoral accumulation of FITC-dextran (molecular weight 2 MDa). The FITC signal (green) was reduced in the FGF-2 co-administered group. Nuclei were stained with DAPI (blue). scale bar: 50 μm

B: Quantification of average fluorescence intensity of FITC-dextran. The signal was significantly lower in FGF-2 co-administered group. Data were expressed as relative value to the average of control group. error bars: mean ± SE, n = 5 each, **: $p < 0.01$

The accumulation of the macromolecules within the tumor is, however, not only influenced by fibrosis. We have previously reported that pericyte coverage of tumor vasculature impairs intratumoral accumulation of doxorubicin-encapsulated micelles in a

BxPC-3 subcutaneous xenograft model [11]. Therefore, we investigated whether FGF-2 could influence vascular density and pericyte coverage of tumor vasculature, but no significant differences were observed in PECAM1 and α-SMA immunostaining (Figure 5A). Consistently, neither vascular density nor pericyte coverage was significantly different between the two groups (Figure 5B and C).

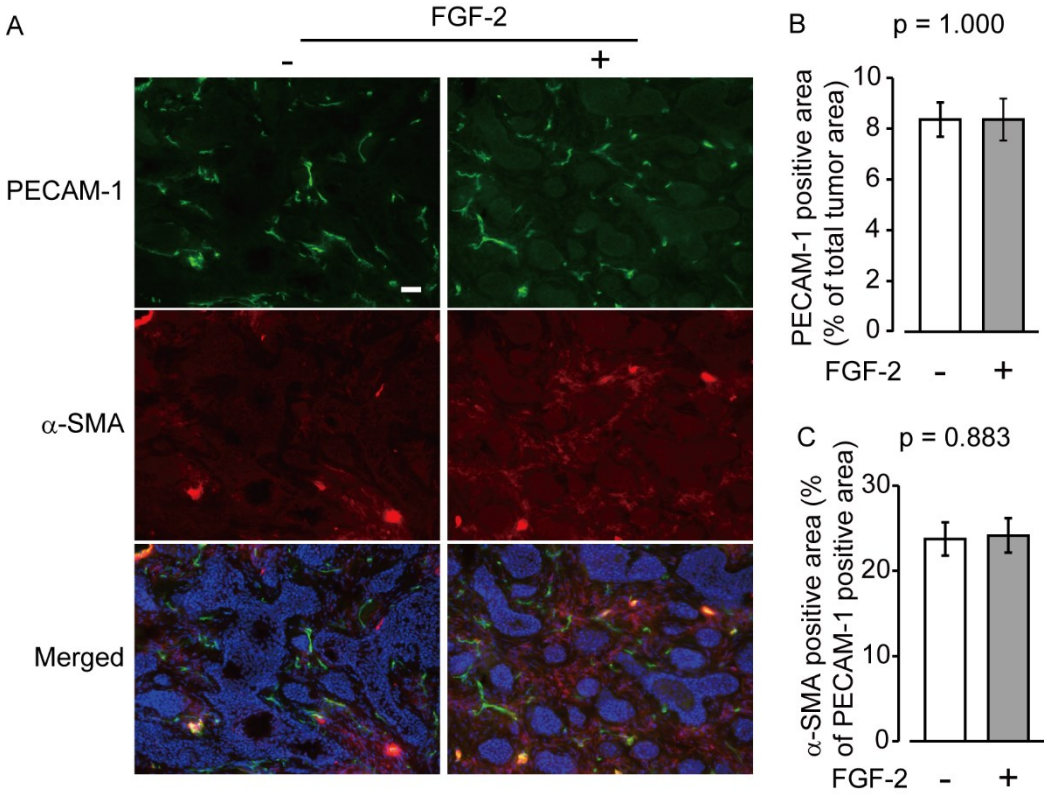


**Figure 5 FGF-2 did not affect vascular density and pericyte coverage**

A: Representative photographs of PECAM-1 and α-SMA staining. No clear differences were observed. Blue indicates nuclei (DAPI). Scale bar: 50 μm

B: Quantification of the rates of PECAM-1 positive areas and PECAM-1/α-SMA double positive areas. No significant differences were observed. Error bars: mean ± SE, n = 5 each.

FGF-2 is also known to promote lymphangiogenesis [20,21]. Relative scarcity of lymphatic vessels is thought to be a factor influencing intratumoral accumulation of macromolecules according to the enhanced permeability and retention (EPR) effect, in addition to leaky tumor vasculature [22,23]. Therefore, we stained tumor samples for LYVE-1, a well-known marker of lymphatic endothelial cells (Figure 6A). FGF-2 significantly increased the density of lymphatic vessels within the tumor (Figure 6B). This was somewhat in contradiction to our expectations, since FGF-2 co-administration showed less, not more, accumulation of FITC-dextran. However, the frequency of lymphatic vessels with conspicuous lumen was significantly lower in the FGF-2 co-administered group (Figure 6C), which may explain this discordance. These findings overall indicate that changes in lymphangiogenesis do not necessarily contribute to the decrease in intratumoral accumulation of FITC-dextran in the FGF-2 co-administered BxPC-3 subcutaneous xenograft model.

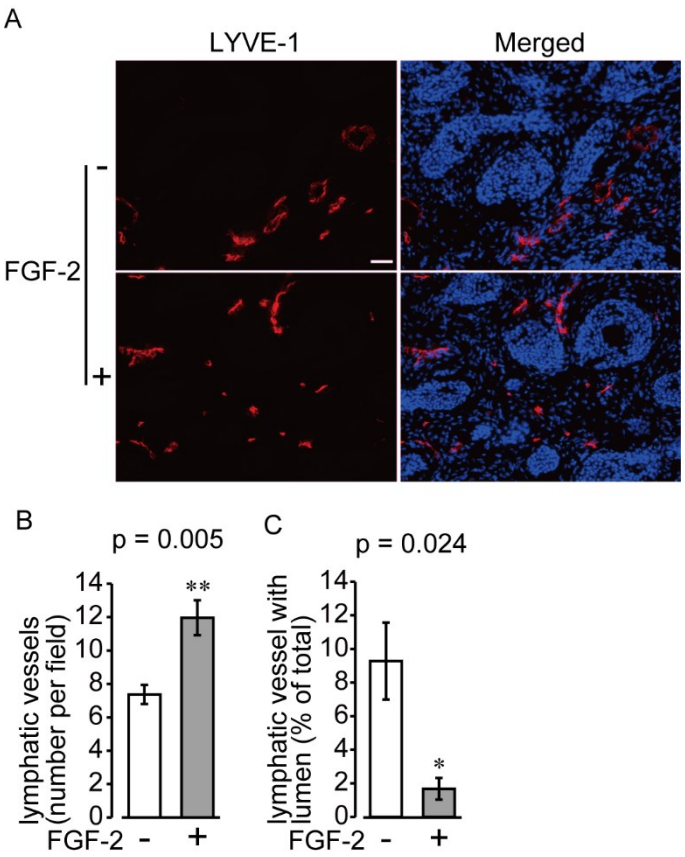


**Figure 6 FGF-2 promoted lymphangiogenesis in a BxPC-3 xenograft model.**

A: Representative photographs of LYVE-1 staining. More lymphatic vessels were observed in the FGF-2 co-administered group, but less lymphatic vessels with conspicuous lumen were observed in the FGF-2 co-administered group. scale bar: 50 μm

B: Quantification of intratumoral lymphatic vessel density. FGF-2 significantly increased lymphatic vessel density. error bars: mean ± SE, n = 5 each, *: $p < 0.05$

C: Quantification of the frequency of lymphatic vessels with conspicuous lumen. FGF-2 significantly decreased this frequency. error bars: mean ± SE, n = 5 each, *: $p < 0.05$

## Discussion

In this study, we have shown that co-administration of FGF-2 augmented fibrosis in the BxPC-3 subcutaneous xenograft model. Further characterization of this model with enhanced fibrosis revealed that FGF-2 co-administration significantly increased intratumoral collagen deposition (Figure 2), while it did not clearly affect intratumoral hyaluronan accumulation (Figure 3), intratumoral vascular density or pericyte coverage of tumor vasculature (Figure 5). These results suggest that FGF-2 impaired intratumoral accumulation of FITC-dextran mainly by increasing intratumoral collagen deposition in our BxPC-3 subcutaneous xenograft model.

Recently, nab-paclitaxel, a macromolecular formulation of paclitaxel bound to albumin, has been successful in clinical treatment of pancreatic cancer [24–26]. Although the formulation is a macromolecule of 130 nm in diameter before administration, the drug may soon decay to around a size of a single albumin molecule in the bloodstream [27–29]. It is therefore not clear whether the results of this study using dextran of 2 MDa may immediately be applicable to predict the behavior of nab-paclitaxel in fibrotic tumor tissue. Furthermore, the pharmacokinetics of albumin-bound molecules, including nab-paclitaxel, is not just a function of particle size but also of interactions with proteins *in vivo* such as secreted protein acidic and rich in cysteine (SPARC) [30]. The latter factor

is an interesting topic which warrants further studies.

As the mechanism of increased fibrosis by FGF-2, previous reports have shown that FGF-2 promoted infiltration of immune cells in Matrigel plug assays [31,32]. Another group has shown that subcutaneous injection of FGF-2 augmented fibrosis via up-regulation of monocyte/macrophage chemoattractant protein-1 (MCP-1) and increased infiltration of immune cells, such as macrophages, in newborn C57BL/6 mice [33]. Also, macrophages are known to induce fibrosis in several organs, such as heart and kidney. Our results suggest that collagen was derived from host stromal cells (Figure 2), but the precise mechanisms underlying FGF-2 enhanced fibrosis in our model remain to be elucidated.

We have shown in this study using our new model that accumulation of macromolecule was less in the fibrosis-increased condition. However, factors which may explain the decrease in macromolecular accumulation other than the increase in the amount of fibrosis per se can be envisaged. First, interstitial fluid pressure (IFP) is a factor known to regulate intratumoral accumulation of anti-tumor drugs and is reported to be often increased in solid tumors [34–36]. Previous reports have shown that systemic administration of collagenase to tumor-bearing mice decreased intratumoral IFP and improved intratumoral accumulation of monoclonal antibodies and cationic liposomes

[6,7]. Therefore, enhanced fibrosis may act indirectly via an increase in intratumoral IFP *in vivo*. On the other hand, collagen may also be a physical barrier against intratumoral accumulation of macromolecular drugs because an *in vitro* study, in which IFP is not involved, has shown that treatment of spheroids of tumor cells with collagenase improved penetration of polyethylene nanospheres into the spheroids [8]. These suggest that increased IFP, in concert with the physical barrier posed by collagen bundles, may impede diffusion of macromolecular anti-tumor drugs into stromal areas.

It is unclear from the present study whether changes in lymphangiogenesis, another potential factor as posited by the theory of the EPR effect [22,23], induced by FGF-2 co-administration influenced accumulation of macromolecules. Though previous studies have shown that interstitial fluid exits tissue through normal lymphatic vessels [20], it has not yet been clearly shown whether change in intratumoral lymphatic vessel can directly affect the intratumoral accumulation of macromolecules. That FGF-2 co-administration promoted lymphangiogenesis in the BxPC-3 xenograft model at least in terms of LYVE-1 positive vessel density (Figure 6) was consistent with previous reports *in vivo* [21,37]. However, FGF-2 decreased the frequency of lymphatic vessels with conspicuous lumen, which may indicate an increase in collapsed lymphatic vessels within the tumor. Previous studies have indicated that intratumoral lymphatic vessels were non-

functional [38]. These findings therefore suggest that increase of lymphangiogenesis in FGF-2-treated condition did not contribute to the intratumoral accumulation of FITC-dextran. Further experiments such as ferritin microlymphangiography [39] may be necessary to evaluate the function of lymphatic vessels in this model.

In summary, we have established a novel murine pancreatic cancer model with enhanced fibrosis by co-administering FGF-2 in the BxPC-3 subcutaneous xenograft model. The model we have established provides a preclinical model to predict intratumoral accumulation of macromolecules and to evaluate efficacy of drugs targeting the tumor stroma, especially in tumors with extensive fibrosis.

**Acknowledgements**

This study was supported by KAKENHI (23790433 and 26293119), Health Labor Sciences Research Grant, and granted also by the Japan Society for the Promotion of Science (JSPS) through the “Funding Program for World-Leading Innovative R&D on Science and Technology (FIRST Program),” initiated by the Council for Science and Technology Policy (CSTP). We thank Dr. Hiroyoshi Y. Tanaka for his critical reading of the work.

## References


[1] M. Schober, R. Jesenofsky, R. Faissner, C. Weidenauer, W. Hagmann, P. Michl, et al., Desmoplasia and chemoresistance in pancreatic cancer., Cancers (Basel). 6 (2014) 2137–54. doi:10.3390/cancers6042137.

[2] M. Erkan, S. Hausmann, C.W. Michalski, A.A. Fingerle, M. Dobritz, J. Kleeff, et al., The role of stroma in pancreatic cancer: diagnostic and therapeutic implications., Nat. Rev. Gastroenterol. Hepatol. 9 (2012) 454–67. doi:10.1038/nrgastro.2012.115.

[3] A.A. Rucki, L. Zheng, Pancreatic cancer stroma: understanding biology leads to new therapeutic strategies., World J. Gastroenterol. 20 (2014) 2237–46. doi:10.3748/wjg.v20.i9.2237.

[4] P.P. Provenzano, C. Cuevas, A.E. Chang, V.K. Goel, D.D. Von Hoff, S.R. Hingorani, Enzymatic targeting of the stroma ablates physical barriers to treatment of pancreatic ductal adenocarcinoma., Cancer Cell. 21 (2012) 418–29. doi:10.1016/j.ccr.2012.01.007.

[5] M.A. Jacobetz, D.S. Chan, A. Neesse, T.E. Bapiro, N. Cook, K.K. Frese, et al., Hyaluronan impairs vascular function and drug delivery in a mouse model of pancreatic cancer., Gut. 62 (2013) 112–20. doi:10.1136/gutjnl-2012-302529.

[6] L. Eikenes, Collagenase Increases the Transcapillary Pressure Gradient and Improves the Uptake and Distribution of Monoclonal Antibodies in Human Osteosarcoma Xenografts, Cancer Res. 64 (2004) 4768–4773. doi:10.1158/0008-5472.CAN-03-1472.

[7] M. Kato, Y. Hattori, M. Kubo, Y. Maitani, Collagenase-1 injection improved tumor distribution and gene expression of cationic lipoplex., Int. J. Pharm. 423 (2012) 428–34. doi:10.1016/j.ijpharm.2011.12.015.

[8] T.T. Goodman, P.L. Olive, S.H. Pun, Increased nanoparticle penetration in collagenase-treated multicellular spheroids., Int. J. Nanomedicine. 2 (2007) 265–74.

[9] M. Erkan, C. Reiser-Erkan, C.W. Michalski, B. Kong, I. Esposito, H. Friess, et al., The impact of the activated stroma on pancreatic ductal adenocarcinoma biology and therapy resistance., Curr. Mol. Med. 12 (2012) 288–303.

[10] R.A. Weinberg, Dialogue Replaces Monologue: Heterotypic Interactions and the Biology of Angiogenesis, in: Chapter 13, The Biology of Cancer, Second Ed., Garland Science, New York, NY, USA, 2013: pp. 577–640.

[11] M.R. Kano, Y. Bae, C. Iwata, Y. Morishita, M. Yashiro, M. Oka, et al., Improvement of cancer-targeting therapy, using nanocarriers for intractable solid tumors by inhibition of TGF-beta signaling., Proc Natl Acad Sci U S A. 104 (2007) 3460–5. doi:10.1073/pnas.0611660104.

[12] H. Hosoya, K. Kadowaki, M. Matsusaki, H. Cabral, H. Nishihara, H. Ijichi, et al., Engineering fibrotic tissue in pancreatic cancer: A novel three-dimensional model to investigate nanoparticle delivery., Biochem Biophys Res Commun. 419 (2012) 32–7. doi:10.1016/j.bbrc.2012.01.117.

[13] H. Kuniyasu, J.L. Abbruzzese, K.R. Cleary, I.J. Fidler, Induction of ductal and stromal hyperplasia by basic fibroblast growth factor produced by human pancreatic carcinoma., Int. J. Oncol. 19 (2001) 681–5.

[14] A. Masamune, T. Watanabe, K. Kikuta, T. Shimosegawa, Roles of pancreatic stellate cells in pancreatic inflammation and fibrosis., Clin. Gastroenterol. Hepatol. 7 (2009) S48–54. doi:10.1016/j.cgh.2009.07.038.

[15] S. Lunardi, R.J. Muschel, T.B. Brunner, The stromal compartments in pancreatic cancer: are there any therapeutic targets?, Cancer Lett. 343 (2014) 147–55. doi:10.1016/j.canlet.2013.09.039.

[16] E. Schneider, A. Schmid-Kotsas, J. Zhao, H. Weidenbach, R.M. Schmid, A. Menke, et al., Identification of mediators stimulating proliferation and matrix synthesis of rat pancreatic stellate cells., Am. J. Physiol. Cell Physiol. 281 (2001) C532–43.

[17] M.G. Bachem, M. Schünemann, M. Ramadani, M. Siech, H. Beger, A. Buck, et al., Pancreatic carcinoma cells induce fibrosis by stimulating proliferation and matrix synthesis of stellate cells., Gastroenterology. 128 (2005) 907–21.

[18] N. Blumenkrantz, G. Asboe-Hansen, A quick and specific assay for hydroxyproline, Anal. Biochem. 55 (1973) 288–291. doi:10.1016/0003-2697(73)90316-3.

[19] M.R. Kano, Y. Komuta, C. Iwata, M. Oka, Y. Shirai, Y. Morishita, et al., Comparison of the effects of the kinase inhibitors imatinib, sorafenib, and transforming growth factor-beta receptor inhibitor on extravasation of nanoparticles from neovasculature., Cancer Sci. 100 (2009) 173–80. doi:10.1111/j.1349-7006.2008.01003.x.

[20] S.A. Stacker, S.P. Williams, T. Karnezis, R. Shayan, S.B. Fox, M.G. Achen, Lymphangiogenesis and lymphatic vessel remodelling in cancer., Nat. Rev. Cancer. 14 (2014) 159–72. doi:10.1038/nrc3677.

[21] L.K. Chang, G. Garcia-Cardeña, F. Farnebo, M. Fannon, E.J. Chen, C. Butterfield, et al., Dose-dependent response of FGF-2 for lymphangiogenesis., Proc. Natl. Acad. Sci. U. S. A. 101 (2004) 11658–63. doi:10.1073/pnas.0404272101.

[22] Y. Matsumura, H. Maeda, A new concept for macromolecular therapeutics in cancer chemotherapy: mechanism of tumoritropic accumulation of proteins and the antitumor agent smancs., Cancer Res. 46 (1986) 6387–92.

[23] J. Fang, H. Nakamura, H. Maeda, The EPR effect: Unique features of tumor blood vessels for drug delivery, factors involved, and limitations and augmentation of the effect., Adv Drug Deliv Rev. 63 (2011) 136–51. doi:10.1016/j.addr.2010.04.009.

[24] D.D. Von Hoff, R.K. Ramanathan, M.J. Borad, D.A. Laheru, L.S. Smith, T.E. Wood, et al., Gemcitabine plus nab-paclitaxel is an active regimen in patients with advanced pancreatic cancer: a phase I/II trial., J. Clin. Oncol. 29 (2011) 4548–54. doi:10.1200/JCO.2011.36.5742.

[25] A. Gaitanis, S. Staal, Liposomal doxorubicin and nab-paclitaxel: nanoparticle cancer chemotherapy in current clinical use., Methods Mol Biol. 624 (2010) 385–92. doi:10.1007/978-1-60761-609-2_26.

[26] D.D. Von Hoff, T. Ervin, F.P. Arena, E.G. Chiorean, J. Infante, M. Moore, et al., Increased survival in pancreatic cancer with nab-paclitaxel plus gemcitabine., N. Engl. J. Med. 369 (2013) 1691–703. doi:10.1056/NEJMoa1304369.

[27] Taiho Pharmaceutical Co. Ltd., Abraxane® i.v. infusion 100 mg, Interview Form, 2014.

[28] A. Sparreboom, C.D. Scripture, V. Trieu, P.J. Williams, T. De, A. Yang, et al., Comparative preclinical and clinical pharmacokinetics of a cremophor-free, nanoparticle albumin-bound paclitaxel (ABI-007) and paclitaxel formulated in Cremophor (Taxol)., Clin. Cancer Res. 11 (2005) 4136–43. doi:10.1158/1078-0432.CCR-04-2291.

[29] N. Desai, V. Trieu, Z. Yao, L. Louie, S. Ci, A. Yang, et al., Increased antitumor activity, intratumor paclitaxel concentrations, and endothelial cell transport of cremophor-free, albumin-bound paclitaxel, ABI-007, compared with cremophor-based paclitaxel., Clin. Cancer Res. 12 (2006) 1317–24. doi:10.1158/1078-0432.CCR-05-1634.

[30] D.A. Yardley, nab-Paclitaxel mechanisms of action and delivery., J. Control. Release. 170 (2013) 365–72. doi:10.1016/j.jconrel.2013.05.041.

[31] D. Leali, P. Dell'Era, H. Stabile, B. Sennino, A.F. Chambers, A. Naldini, et al., Osteopontin (Eta-1) and fibroblast growth factor-2 cross-talk in angiogenesis., J. Immunol. 171 (2003) 1085–93.

[32] A. Passaniti, R.M. Taylor, R. Pili, Y. Guo, P. V Long, J.A. Haney, et al., A simple, quantitative method for assessing angiogenesis and antiangiogenic agents using reconstituted basement membrane, heparin, and fibroblast growth factor., Lab. Invest. 67 (1992) 519–28.

[33] S. Chujo, F. Shirasaki, M. Kondo-Miyazaki, Y. Ikawa, K. Takehara, Role of connective tissue growth factor and its interaction with basic fibroblast growth factor and macrophage chemoattractant protein-1 in skin fibrosis., J. Cell. Physiol. 220 (2009) 189–95. doi:10.1002/jcp.21750.

[34] R.K. Jain, Transport of molecules in the tumor interstitium: a review., Cancer Res. 47 (1987) 3039–51.

[35] C.-H. Heldin, K. Rubin, K. Pietras, A. Ostman, High interstitial fluid pressure - an obstacle in cancer therapy., Nat Rev Cancer. 4 (2004) 806–13. doi:10.1038/nrc1456.

[36] S.J. Lunt, T.M. Kalliomaki, A. Brown, V.X. Yang, M. Milosevic, R.P. Hill, Interstitial fluid pressure, vascularity and metastasis in ectopic, orthotopic and spontaneous tumours., BMC Cancer. 8 (2008) 2. doi:10.1186/1471-2407-8-2.

[37] R. Cao, A. Eriksson, H. Kubo, K. Alitalo, Y. Cao, J. Thyberg, Comparative evaluation of FGF-2-, VEGF-A-, and VEGF-C-induced angiogenesis, lymphangiogenesis, vascular fenestrations, and permeability., Circ. Res. 94 (2004) 664–70. doi:10.1161/01.RES.0000118600.91698.BB.

[38] T.P. Padera, A. Kadambi, E. di Tomaso, C.M. Carreira, E.B. Brown, Y. Boucher, et al., Lymphatic metastasis in the absence of functional intratumor lymphatics., Science. 296 (2002) 1883–6. doi:10.1126/science.1071420.

[39] A.J. Leu, D.A. Berk, A. Lymboussaki, K. Alitalo, R.K. Jain, Absence of Functional Lymphatics within a Murine Sarcoma: A Molecular and Functional Evaluation, Cancer Res. 60 (2000) 4324–4327.